Article

Cell Metabolism

Caloric Restriction Leads to Browning of White Adipose Tissue through Type 2 Immune Signaling

Graphical Abstract

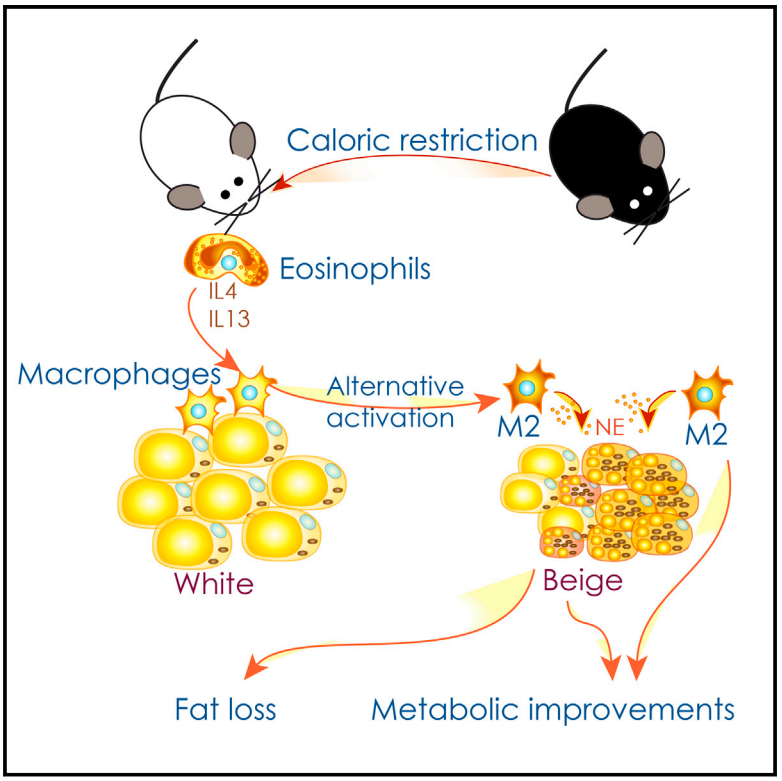

Authors

Salvatore Fabbiano, Nicolas Suárez-Zamorano, Dorothée Rigo, Christelle Veyrat-Durebex, Ana Stevanovic Dokic, Didier J. Colin, Mirko Trajkovski

Correspondence

mirko.trajkovski@unige.ch

In Brief

Fabbiano et al. demonstrate that caloric restriction promotes functional beige fat development via enhanced type 2 immune response and SIRT1 expression in macrophages. Genetic suppression of type 2 cytokine signaling prevents browning and subcutaneous fat loss, and it abrogates the metabolic improvements elicited by caloric restriction.

Highlights

- Caloric restriction leads to preferential glucose uptake in white fat
- Caloric restriction promotes the development of functional beige fat
- Decreased caloric intake enhances type 2 immune response and SIRT1 expression
- Type 2 signaling is necessary for the browning and the metabolic improvements during CR

Fabbiano et al., 2016, Cell Metabolism *24*, 434–446
September 13, 2016
http://dx.doi.org/10.1016/j.cmet.2016.07.023

CellPress

Cell Metabolism
Article

Caloric Restriction Leads to Browning of White Adipose Tissue through Type 2 Immune Signaling

Salvatore Fabbiano,[1,2] Nicolas Suárez-Zamorano,[1,2] Dorothée Rigo,[1,2] Christelle Veyrat-Durebex,[1,2] Ana Stevanovic Dokic,[1,2] Didier J. Colin,[3] and Mirko Trajkovski[1,2,4,5,*]

[1]Department of Cell Physiology and Metabolism, Centre Médical Universitaire (CMU), Faculty of Medicine, University of Geneva, 1211 Geneva, Switzerland

[2]Diabetes Centre, Faculty of Medicine, University of Geneva, 1211 Geneva, Switzerland

[3]Centre for BioMedical Imaging (CIBM), University Hospitals of Geneva, 1211 Geneva, Switzerland

[4]Institute for Genetics and Genomics in Geneva (iGE3), University of Geneva, 1211 Geneva, Switzerland

[5]Lead Contact

*Correspondence: mirko.trajkovski@unige.ch

http://dx.doi.org/10.1016/j.cmet.2016.07.023

SUMMARY

Caloric restriction (CR) extends lifespan from yeast to mammals, delays onset of age-associated diseases, and improves metabolic health. We show that CR stimulates development of functional beige fat within the subcutaneous and visceral adipose tissue, contributing to decreased white fat and adipocyte size in lean C57BL/6 and BALB/c mice kept at room temperature or at thermoneutrality and in obese leptin-deficient mice. These metabolic changes are mediated by increased eosinophil infiltration, type 2 cytokine signaling, and M2 macrophage polarization in fat of CR animals. Suppression of the type 2 signaling, using *Il4ra*$^{-/-}$, *Stat6*$^{-/-}$, or mice transplanted with *Stat6*$^{-/-}$ bone marrow-derived hematopoietic cells, prevents the CR-induced browning and abrogates the subcutaneous fat loss and the metabolic improvements induced by CR. These results provide insights into the overall energy homeostasis during CR, and they suggest beige fat development as a common feature in conditions of negative energy balance.

INTRODUCTION

Brown adipose tissue (BAT) catabolizes lipids to produce heat, a function that is mediated by the tissue-specific uncoupling protein 1 (UCP1). BAT differentiation can be induced by prolonged cold exposure and beta-adrenergic stimulation, which leads to elevated intracellular cyclic AMP (Cannon and Nedergaard, 2004; Himms-Hagen et al., 2000; Young et al., 1984) and thyroid hormones, necessary for full *Ucp1* mRNA expression (Bianco and Silva, 1987; Silva, 1988). The BAT is present at distinct anatomical sites, including the interscapular, perirenal, and axillary depots. Brown fat cells also emerge in inguinal subcutaneous white adipose tissue (WAT) (ingSAT), known as beige cells in, a process referred to as browning. Loss of BAT function is linked to obesity and metabolic diseases (Lowell et al., 1993). Increased beige and brown fat development, on the other hand, increases energy expenditure and improves insulin sensitivity (Stanford et al., 2013). Experimental increases of BAT in animals are associated with a lean and healthy phenotype (Ghorbani et al., 1997; Guerra et al., 1998; Kopecky et al., 1995), suggesting the manipulation of the fat stores as an anti-obesity therapeutic perspective. Browning appears consequent to physiological stimuli, such as cold exposure or endurance exercise (Cousin et al., 1992; Guerra et al., 1998; Himms-Hagen et al., 2000). In addition to the physiological stimuli, also microbiota depletion (Suárez-Zamorano et al., 2015; Chevalier et al., 2015) and Roux-en-Y gastric bypass weight-loss surgery (RYGB) (Neinast et al., 2015) promote the development of beige fat. It remains unclear whether there is a common feature between these seemingly unrelated physiological and interventional stimuli that could lead to the beige fat development.

A common characteristic of all the above conditions that lead to browning is the negative energy balance: the energy uptake is lower than the energy expenditure, resulting in weight loss primarily due to the decreased fat mass. Caloric restriction (CR) is a classical example of energy scarcity. CR up to 40% of nutritious diet intake extends healthy lifespan from yeast to mammals (Colman et al., 2014; Wei et al., 2008), delays the onset of multiple age-associated diseases, and improves metabolic health (De Guzman et al., 2013; Ocampo et al., 2012). The beneficial effects of CR are chiefly mediated by the reduced energy intake, which affects the ration of cellular substrates, such as NAD^+/NAD and AMP/ATP, and triggers downstream changes in several energy-sensing pathways (Cantó and Auwerx, 2011). We hypothesized that energy scarcity could be a physiological trigger that drives the browning of the white fat. In this study, we found that CR promotes functional beige fat development. We show that the browning is concomitant with the increased type 2 cytokine signaling and that this signaling is necessary for the beige fat development, for the decrease of the subcutaneous fat, and for many of the metabolic improvements caused by the CR. Genetic suppression of the type 2 cytokine signaling during CR abrogates the white fat browning, lowers the energy expenditure of the CR mice, prevents the subcutaneous fat loss, and ablates the improved insulin sensitivity and glucose tolerance caused by the CR. Our data suggest that white fat browning through enhanced type 2 signaling is a common feature of conditions of negative energy balance.

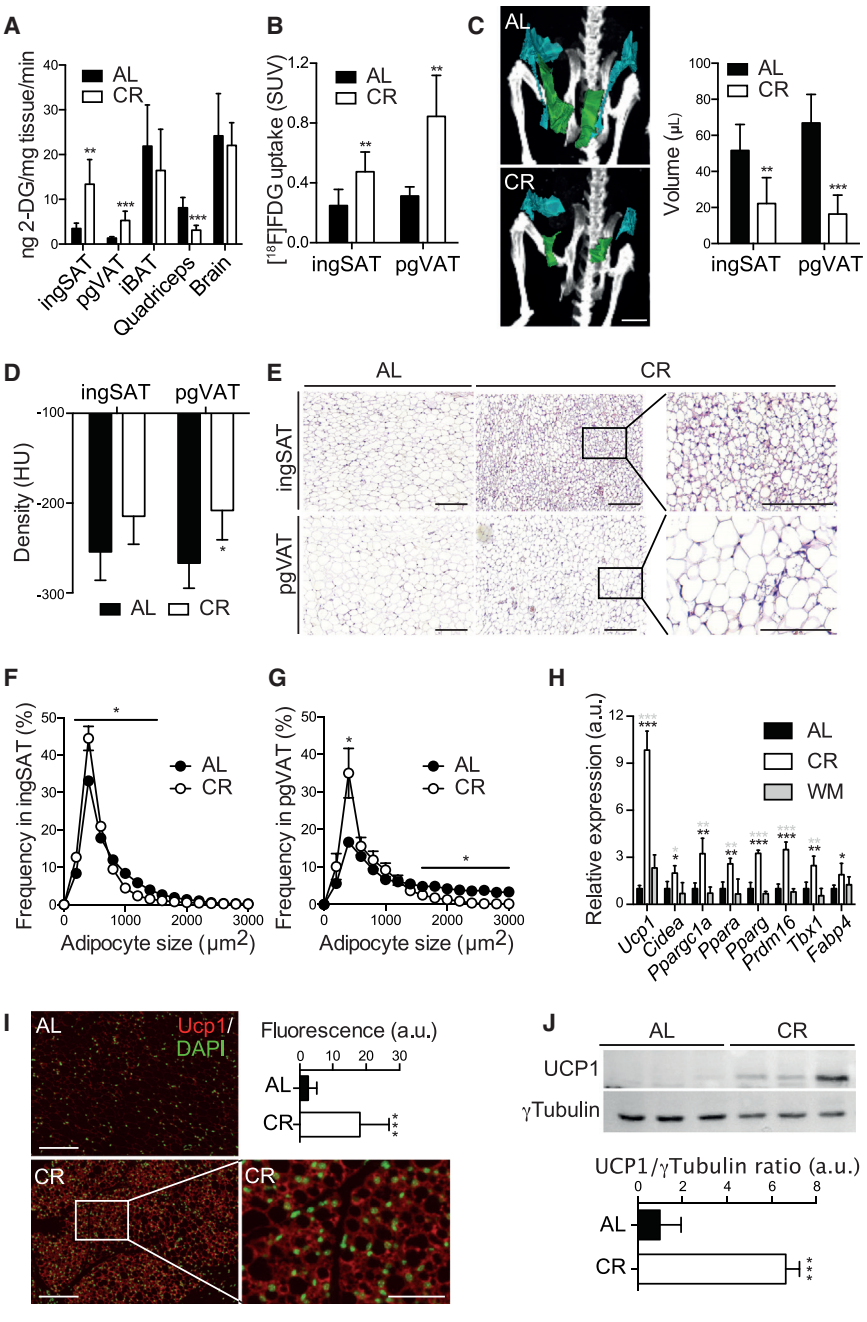

Figure 1. Caloric Restriction Promotes Browning of WAT

(A) 2[^{14}C]deoxyglucose (2[^{14}C]-DG) uptake in ad libitum (AL) and caloric restricted (CR) mice in the indicated organs (n = 6 per group) is shown.

(B) Standardized uptake values (SUVs) of radiolabeled tracer 2-deoxy-2-[^{18}F]fluoro-D-glucose ([^{18}F]FDG) in ingSAT and pgVAT of AL and CR mice (n = 6 per group) were revealed using PET-CT.

(C) 3D reconstitution of ingSAT and pgVAT using the PET-CT scans (left) from mice as in (B) and corresponding quantifications of the total ingSAT and pgVAT volumes (right) are shown. Scale bar, 2.5 mm.

(D) IngSAT and pgVAT density are shown in Hounsfield units from mice as in (B).

(E) Representative H&E-stained histological sections from ingSAT and pgVAT of AL and CR mice are shown. Scale bar, 200 μm.

(F and G) Cell size profiling of adipocytes from ingSAT (F) and pgVAT (G) of AL and CR mice (n = 6 per group). Adipocyte size measurements were done on two sections per mouse.

(H) Relative mRNA expression of browning markers in ingSAT of AL, CR, and weight-matched (WM) mice (n = 6) is shown.

(I) Representative images (left) and corresponding whole-section quantification (right) of immunofluorescent stainings of Ucp1 protein in ingSAT (n = 6 per group) are shown.

(J) Representative western blot (top) and quantification (bottom) of protein lysates from ingSAT of AL and CR mice are shown.

Mice were tested after 4 weeks of CR. Error bars show mean ± SD. Significance was calculated using non-paired two-tailed Student's t test (*p ≤ 0.05, **p ≤ 0.01, and ***p ≤ 0.001).

RESULTS

CR Leads to Preferential Glucose Uptake in White Fat

To investigate the effect of CR on glucose homeostasis, we limited the daily food availability for 40% and found decreased body weight, improved glucose tolerance after an oral glucose load, and increased insulin sensitivity following CR compared to ad libitum (AL)-fed C57BL/6J control wild-type (WT) mice (Figures S1A–S1C). This is in agreement with the previous studies (Barzilai et al., 1998; Barzilai and Gabriely, 2001; Kelley et al., 1993) where the improved insulin sensitivity after CR was attributed in part to suppressed hepatic glucose production.

To examine the peripheral glucose uptake, we administered 2-[^{14}C]deoxyglucose (2-DG) at basal conditions, and we found increased glucose disposal in ingSAT and perigonadal visceral adipose tissue (pgVAT), but no changes in the interscapular BAT (iBAT) and brain and a decrease in the quadriceps muscle (Figure 1A), despite the latter showing increased uptake under insulin-stimulated conditions (Figure S1D). These results suggest that the white fat depots are major glucose disposal tissues in basal conditions, which were further corroborated using positron emission tomography-computed tomography (PET-CT). Specifically, 2-deoxy-2-[^{18}F]fluorodeoxyglucose ([^{18}F]FDG) uptake was increased in the ingSAT and pgVAT, but not in the quadriceps muscle, further suggesting preferential glucose uptake in the white fat depots of CR mice (Figure 1B). Three-dimensional (3D) reconstitution of the CT images demonstrated that CR mice had decreased volumes of their ingSAT and pgVAT depots (Figure 1C). This was accompanied by lower ingSAT, pgVAT, and liver weights, without changes in iBAT, quadriceps muscle, and stomach (Figure S1E).

To investigate whether the changes in the fat volume could be attributed in part to differences in its density, we measured the Hounsfield units on the PET-CT scans. The results revealed that CR mice had higher ingSAT and pgVAT density compared to controls (Figure 1D). These results demonstrate that CR leads to preferential glucose uptake in white fat and that these fat depots in the CR mice are smaller in size and with increased density.

CR Promotes the Development of Functional Beige Fat

To determine whether the higher density and the decreased fat amount are originating from the differences in the adipocyte volume, we measured the adipocyte size distribution using high-content imaging. CR mice had a higher number of small adipocytes with multilocular appearence and a lower number of large adipocytes in both ingSAT and pgVAT depots compared to the AL control animals (Figures 1E–1G), but not in the iBAT of the same animals (Figures S1F and S1G). The fat tissues excised from the CR mice were darker in appearance (Figure S1H). These features are characteristic of mature beige adipocytes. Therefore, we investigated whether CR could affect the browning of the white fat depots, and we found that CR mice showed a marked increase in the browning markers, such as *Ucp1*, cell death-inducing DFFA-like effector A (*Cidea*), peroxisome proliferator-activated receptor gamma coactivator 1 alpha (*Ppargc1a*), peroxisome proliferator-activated receptor alpha (*Ppara*), peroxisome proliferator-activated receptor gamma (*Pparg*), PR domain containing 16 (*Prdm16*), T-box transcription factor (*Tbx1*), and fatty acid-binding protein 4 (*Fabp4*) in the ingSAT (Figure 1H). Surprisingly, most of them, together with tumor necrosis factor receptor superfamily member 9 (*Tnfrsf9*, or CD137) and transmembrane protein 26 (*Tmem26*), also were increased in the pgVAT depots (Figure S1I), but were not changed in the ingSAT or pgVAT of the weight-matched animals compared to the AL controls (Figures 1H and S1I). The increased browning of ingSAT was confirmed by high-content imaging and western blotting, and it suggested an increased number of Ucp1-positive cells and increased UCP1 protein level in the ingSAT of the CR mice (Figures 1I and 1J).

These data demonstrate that CR promotes browning in WATs. The beige fat was already detected after 1 week of CR, and it further increased or reached its highest levels after 2 or 4 weeks, respectively (Figures S1J, S1K, and 1H). The browning was still present, albeit at lower levels, 2 weeks after the end of the CR, and it was completely reversed 5 weeks after providing food AL to the 4-week CR animals (Figures S1L and S1M). A 48-hr cold exposure led to an ~150-fold increase in the *Ucp1* expression compared to the 60-fold increase in the AL relative to the room temperature (RT) AL controls (Figure S1N), suggesting that the newly developed beige fat is functionally active. This conclusion was further corroborated by oxygen consumption rate (OCR) measurements after isoproterenol stimulation using either the Seahorse analyzer or the Clark electrode. Both methods revealed that adipocytes isolated from the CR mice have greater response to beta-adrenergic stimuli compared to cells from AL mice (Figures 2A and 2B), suggesting increased thermogenic capacity following CR. To further investigate the functional properties of the newly developed beige fat, we measured the glycerol release as an indicator of lipolysis rates in response to beta-adrenergic stimulation. Adipocytes isolated from the ingSAT depots of the CR mice displayed increased glycerol release, which was enhanced after the isoproterenol treatment (Figure 2C), demonstrating an increased lipolysis in response to beta-adrenergic stimulation. Together, these data demonstrate that fat tissues and adipocytes isolated from the CR mice exhibit increased respiratory capacity and lipolysis rates as an important functional characteristic of the beige fat.

To further investigate the in vivo functional importance of the newly developed beige fat, we exposed the mice to acute cold and monitored the eye temperature representative of the internal body temperature, as well as the ventral and dorsal temperatures using infrared imaging (Figure 2D). In these experiments the food was given AL to both groups to exclude the potential role of the acutely consumed food on the cold tolerance. Consistent with previous observations (Ferguson et al., 2007), CR mice had a lower basal temperature compared to the AL controls (Figures S2C–S2E). Despite the lower starting point, the CR mice showed constant temperature for the whole course of the cold exposure, while AL mice dropped their body temperature during the acute cold stress (Figures 2E and S2A–S2E). This was associated with decreased blood glucose levels and a marked increase in food consumption in the CR mice (Figures S2F–S2H). The enhanced energy harvest during acute cold contributes to maintaining the body temperature (Chevalier et al., 2015), while restricting the available food lowers it. Therefore, to exclude that the increased food consumption of the CR mice was the cause for their improved cold tolerance, we limited the food availability during the initial 6 hr of the cold stress. Similar to the results obtained when the food was available AL during the cold, CR mice were more protected from the cold-induced temperature drop when food availability was restricted (Figures 2F and S2I–S2L), suggesting that the increase in the acutely consumed food was not the cause of their improved cold tolerance. Similar results were observed when food was available AL to both groups 24 hr before and during the cold exposure (Figures 2G and S2M–S2O). Together, these results demonstrate that the newly developed beige fat is functionally active.

CR Leads to Browning at Thermoneutrality in Obese Mice and in Mice Fed the CR Diet

We extended our studies to mice kept at thermoneutrality, where the increased browning would be driven by the CR alone, excluding the effect of the environmental temperature (Feldmann et al., 2009). CR administered under thermoneutral conditions led to decreased body weight, increased tolerance to glucose after an oral glucose load, and constant body temperature following acute cold exposure when compared to AL controls kept at thermoneutrality (Figures 3A, S3A, and S3B). Also at thermoneutral conditions, CR lowered the amounts of ingSAT and pgVAT. The adipocytes isolated from the fat depots of the CR mice kept at thermoneutrality were smaller and with multilocular appearance, and they showed increased expression of the browning markers, albeit to a lower magnitude compared to mice kept at RT, consistent with the absence of a mild thermal stimulation (Figures 3B–3D and S3C–S3I). These data suggest that the CR-induced browning does not appear as a result of the decreased thermal isolation due to the decreased fat content of the CR mice.

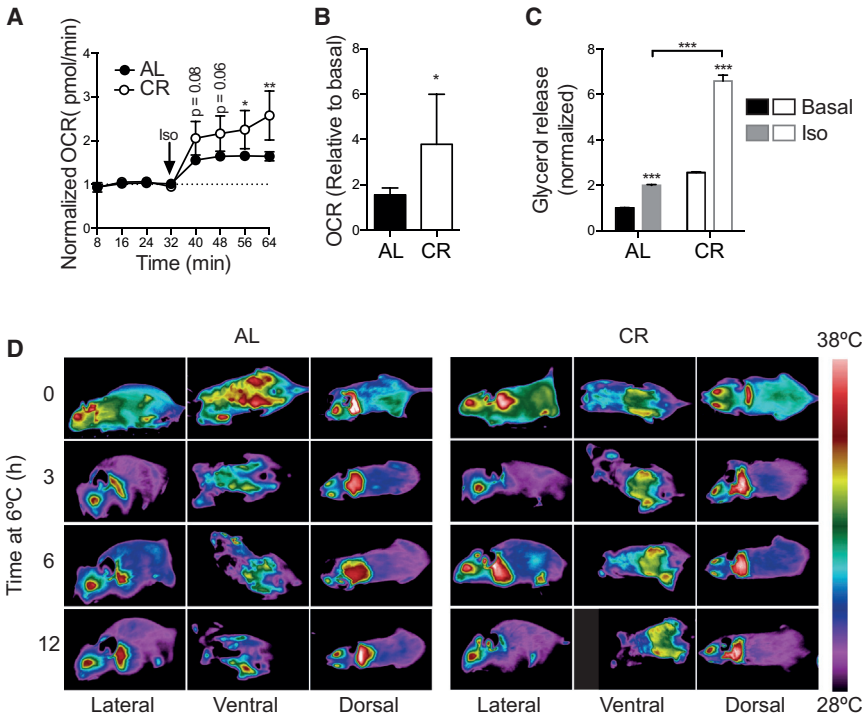

Figure 2. The Developed Beige Fat after CR Shows Increased Thermogenic Capacity

(A) Normalized oxygen consumption rate (OCR) in ingSAT biopsies from AL and CR mice detected with Seahorse analyzer. Iso: isoproterenol (n = 4 mice per group assayed in triplicate).

(B) OCR in ingSAT biopsies of mice as in (A), measured with Clark electrode. Values are shown as ratios between isoproterenol-stimulated and basal conditions (n = 5 per group).

(C) Glycerol release in ingSAT adipocytes from AL and CR mice under basal and isoproterenol-stimulated conditions (n = 4 per group) is shown.

(D) Representative infrared images show AL and CR mice at the indicated time points during 12-hr (h) cold exposure.

(E–G) Infrared eye temperature readings from 12-hr cold-exposed mice with AL access to food during the cold exposure (E, n = 8 per group), fasted for the first 6 hr of cold (F, n = 8 per group), or with AL food access 24 hr before and during the cold exposure (G, n = 8 per group).

Error bars show mean ± SD except for (A), where they represent the SEM. Significance was calculated using non-paired two-tailed Student's t test (*$p \leq 0.05$, **$p \leq 0.01$, and ***$p \leq 0.001$).

Accordingly, CR led to improved sensitivity to insulin in obese, leptin-deficient (*ob/ob*) mice (Figure 3E) and to decreased body weight gain of the CR *ob/ob* mice (Figures S3J). This was associated with improved thermogenic capacity and glucose tolerance of the CR obese mice compared to the AL controls and increased expression of the browning markers (Figures 3F, 3G, S3K, and S3L). This demonstrates that CR enhances the beige fat levels also in obese animals and improves their metabolic fitness. We further investigated whether restricting the calories using a different dietary composition would be important for the browning. A 20% CR using protein-rich calorie-restricted diet (CRD) partially phenocopied the chow CRD-fed animals. Specifically, CRD led to decreased body weight and to improved cold tolerance (Figures S3M and 3H). The CRD-fed mice also showed improved glucose tolerance and smaller multilocular adipocytes in both the ingSAT and pgVAT, resulting in decreased adiposity and increased expression of the browning markers (Figures 3I, 3J, and S3M–S3P). These data suggest that the CR-induced browning is not limited to certain dietary components, but is rather a general phenomenon in conditions of reduced energy uptake.

Decreased Caloric Uptake Enhances Type 2 Immune Response

To gain insight into the mechanisms of browning following CR, we profiled the serum corticosterone (Bordone and Guarente, 2005; Qiang et al., 2012) and the cytokine levels in the ingSAT and pgVAT. While no changes were detected in the corticosterone levels (Figures S4A and S4B), the type 2 cytokines IL-4, IL-5, and IL-13 were markedly up-regulated in both ingSAT and pgVAT of CR mice compared to the AL controls (Figures 4A, S4C, and S4D). Eosinophils and the type 2 cytokines are sufficient to promote beige fat development through alternative activation of M2 macrophages expressing tyrosine hydroxylase (TH) (Ganeshan and Chawla, 2014; Lee et al., 2015; Martinez et al., 2009; Qiu et al., 2014), rate-limiting enzyme in the catecholamine biosynthesis (Nguyen et al., 2011). Indeed, *Th* mRNA and TH protein levels were increased in ingSAT and pgVAT in the CR mice (Figures 4B and S4E).

We therefore focused on the type 2 immune response and detected increased frequency of eosinophils in both fat tissues. This was accompanied by an enhanced macrophage expression of the M2 markers CD301 (or macrophage galactose-type C-type lectin 1), Arginase 1 (ARG1), and TH and decreased levels of the M1 markers CD11c and NOS2, suggesting that the alternatively activated macrophages are associated with the increased browning (Figures 4C–4F, S4E, and S4F). From the IL-4-competent cells recovered from WAT of mice, about 90% are eosinophils (Wu et al., 2011) while the rest are made up of small numbers of basophils, $CD4^+$

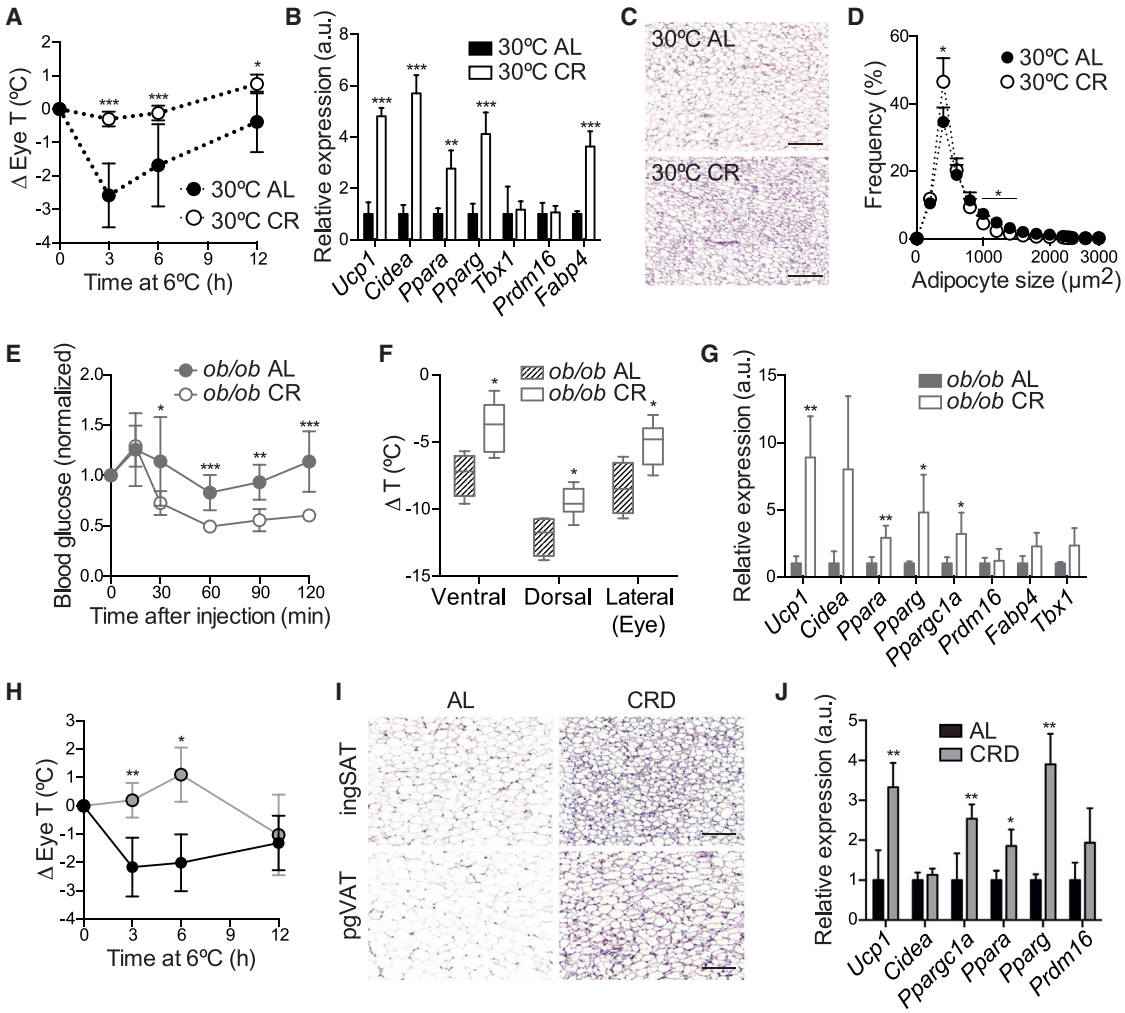

Figure 3. Metabolic Effects of CR in Thermoneutral, Obese, and Animals on CR Diet

(A) Infrared eye temperature readings from 12-hr cold-exposed mice maintained at thermoneutrality since the start of the CR and in the presence of food AL during the cold (n = 6 per group) are shown.

(B) Relative mRNA expression of the indicated browning markers in ingSAT from mice kept at thermoneutrality (n = 6 per group) is shown.

(C and D) Representative histological sections (C) and cell size profiling (D) of ingSAT from mice kept at thermoneutrality (n = 6). Adipocyte size measurements were done on two sections per mouse.

(E–G) Insulin tolerance test (E), infrared temperature readings (F), and mRNA expression in ingSAT (G) of AL-fed and CR *ob/ob* mice (n = 6 per group) are shown.

(H) Eye infrared temperature measurements during a 12-hr cold exposure of AL-fed mice and mice with 20% CR using a calorie-restricted diet (CRD) as specified in the Experimental Procedures (n = 6 per group) are shown.

(I and J) Representative H&E-stained histological sections of AL and CRD mice (I) and relative gene expression of browning markers in ingSAT (J) of mice as in (H) (n = 6 per group) are shown.

Scale bars, 200 μm. Error bars show mean ± SD. Significance was calculated using non-paired two-tailed Student's t test (*$p \leq 0.05$, **$p \leq 0.01$, and ***$p \leq 0.001$).

T cells, and innate lymphoid type 2 cells (ILC2). We therefore also investigated the levels of ILC2 and the $CD4^+$ and $CD8^+$ T cells, and we could not detect changes in their levels following CR (Figures S4K and S4L). In contrast, *Th* mRNA expression also was increased in ingSAT and pgVAT of the CR mice kept at thermoneutrality (Figure 4G). The increase in type 2 response reached a maximum already 1 week after CR, and it was lost after switching CR mice to AL feeding (Figures S5A and S5B).

Type 2 Immune Signaling Is Necessary for the Browning and Metabolic Improvements during CR

To confirm the importance of the type 2 immunity in the CR-induced browning, we used two knockout (KO) animal models, STAT6 (*Stat6*-KO, $Stat6^{-/-}$) and Il4ra ($Il4ra$-KO, $Il4ra^{-/-}$), both models showing impaired type 2 cytokine signaling (Lee et al., 2015; Qiu et al., 2014). The $Il4ra^{-/-}$ animals and their respective controls were on a BALB/c background, while the $Stat6^{-/-}$ mice were on a C57BL/6J background. In both CR KO models, we

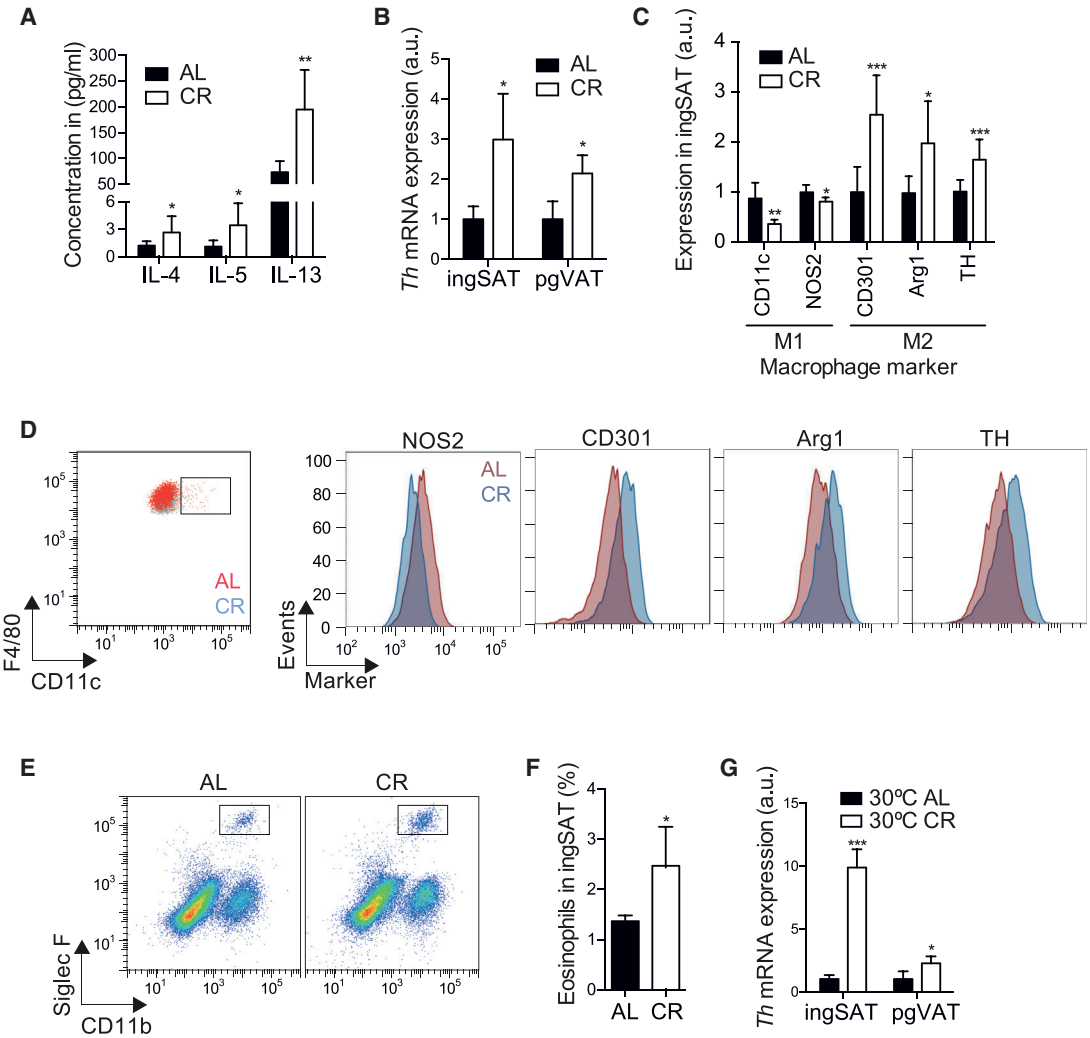

Figure 4. Increased Type 2 Immune Signaling in Fat Tissues of CR Mice

(A) Type 2 cytokine levels in ingSAT of AL and CR mice (n = 8 per group) are shown.

(B) *Th* mRNA levels in ingSAT and pgVAT of mice as in (A) (n = 6 per group) are shown.

(C) Mean fluorescence intensity (MFI) of the indicated M1 and M2 macrophage markers in $CD11b^{+}F4/80^{+}$ cells gated in ingSAT stromal vascular fraction (SVF) of AL and CR mice (n = 6 per group) is shown.

(D) Representative protein expression of M1 and M2 markers in ingSAT macrophages as in (C) is shown.

(E and F) Representative dot plots (E) and corresponding quantifications (F) of $CD11b^{+}$Siglec F^{+} eosinophils in ingSAT SVF of mice as in (A) (n = 6 per group) are shown.

(G) *Th* mRNA levels in ingSAT and pgVAT of AL or CR mice kept at thermoneutrality (30°C) (n = 6 per group) are shown.

Error bars show mean ± SD. Significance was calculated using non-paired two-tailed Student's t test (*$p \leq 0.05$, **$p \leq 0.01$, and ***$p \leq 0.001$).

could not detect improvement in the tolerance to glucose, and we saw milder or no improvement in the sensitivity to insulin in the *Il4ra*$^{-/-}$ and *Stat6*$^{-/-}$ animals, respectively (Figures 5A–5H). Notably, the ingSAT loss during CR was completely prevented in the CR *Stat6*-KO (Figure 5I). Similar to the mice on C57BL/6J background, the calorie-restricted control mice on BALB/c background also decreased their fat weight, while the subcutaneous fat loss was prevented in the CR *Il4ra*-KO mice (Figures 5J, S5C, and S5D). We detected no changes in the [^{18}F]FDG uptake in fat between the CR and AL when we used *Stat6*$^{-/-}$ mice subjected to PET-CT (Figures 5K and S5E), and the ingSAT volume, but not the pgVAT, remained the same between the groups (Figures 5L and 5M). Hounsfied unit measurements revealed no differences in the density of the fat tissues (Figure 5N). These results demonstrate that type 2 signaling is necessary for the metabolic benefits of CR and that its abrogation using either *Stat6*-KO or *Il4ra*-KO animals impairs the reduction in subcutaneous, but not visceral, adiposity under CR.

Suppression of the type 2 signaling ablated the CR-induced increase in M2 macrophages (Figure 6A) and the browning of the white fat depots assessed by measuring the expression of the browning markers (Figures 6B and 6C) and the adipocyte morphology (Figures 6D–6H and S6A–S6E). Since the browning of the fat depots enhances energy dissipation and reduces the

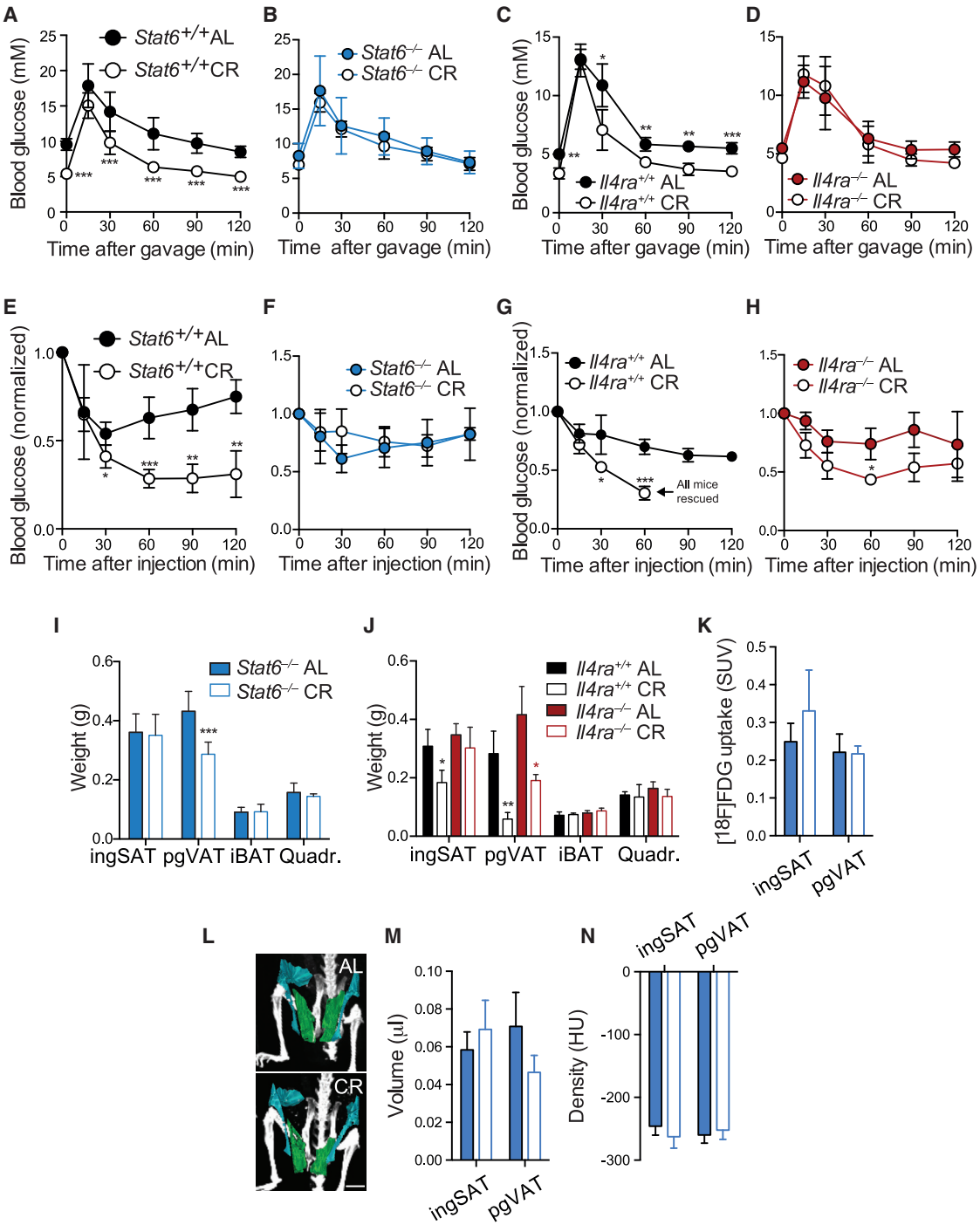

Figure 5. Genetic Suppression of the Type 2 Signaling Ablates the Metabolic Improvements and Subcutaneous Fat Loss Caused by CR

(A–H) Oral glucose tolerance test (OGTT) (A–D) and insulin tolerance test (E–H) of AL and CR *Stat6*$^{+/+}$ (A and E) and *Stat6*$^{-/-}$ (B and F) in the C57BL/6J genetic background and AL and CR *Il4ra*$^{+/+}$ (C and G) and *Il4ra*$^{-/-}$ (D and H) in the BALB/c genetic background (n = 4–6 per group) are shown.

(I and J) Organs weight of AL and CR *Stat6*$^{-/-}$ (I) and *Il4ra*$^{-/-}$ (J) and control *Il4ra*$^{+/+}$ mice on BALB/c genetic background (n = 4–6 per group) are shown.

(K) SUVs of radiolabeled tracer [^{18}F]FDG in ingSAT and pgVAT of AL and CR *Stat6*$^{+/+}$ and *Stat6*$^{-/-}$ mice (n = 5 per group) were revealed using PET-CT.

(L and M) 3D reconstitution of ingSAT and pgVAT using the PET-CT scans (L) from mice as in (K) and corresponding quantifications of the total ingSAT and pgVAT volumes (M) are shown. Scale bar, 2.5 mm.

(N) IngSAT and pgVAT density are shown in Hounsfield units from mice as in (K).

Error bars show mean ± SD. Significance was calculated using non-paired two-tailed Student's t test (*p ≤ 0.05, **p ≤ 0.01, and ***p ≤ 0.001).

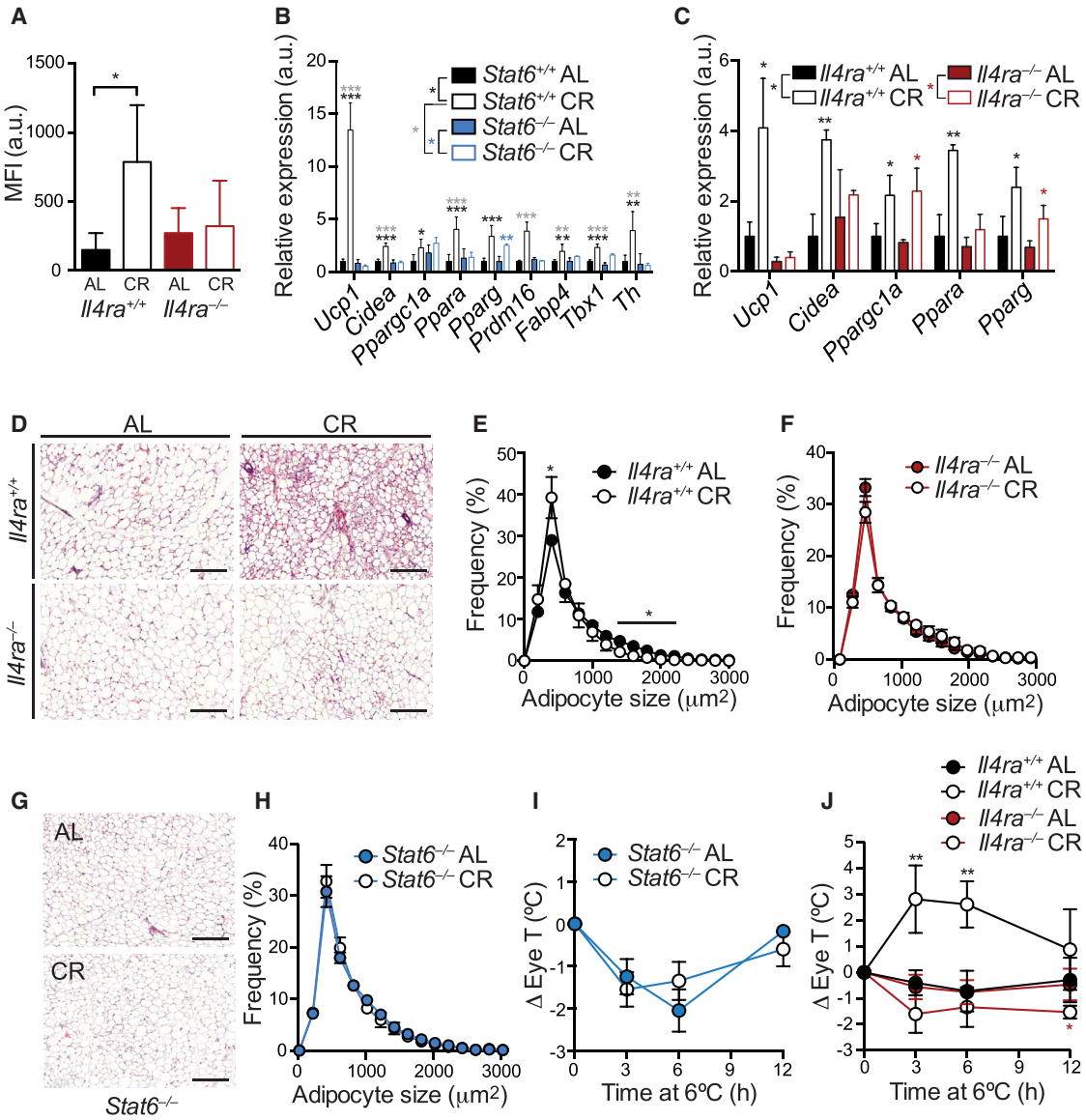

Figure 6. Suppression of the Type 2 Signaling Abrogates the CR-Induced Browning

(A) MFI of CD301 in CD11b$^+$F4/80$^+$ macrophages was detected in ingSAT of AL and CR *Il4ra*$^{+/+}$ and *Il4ra*$^{-/-}$ mice (n = 6 and 4, respectively).

(B and C) Relative mRNA expression of browning markers in ingSAT of AL and CR *Stat6*$^{+/+}$ and *Stat6*$^{-/-}$ (B) and *Il4ra*$^{+/+}$ and *Il4ra*$^{-/-}$ (C) mice (n = 4–6 per group) is shown.

(D–H) Representative H&E-stained histological sections (D and G) and cell size profiling (E, F, and H) in ingSAT of AL and CR *Il4ra*$^{+/+}$ and *Il4ra*$^{-/-}$ (D–F) or *Stat6*$^{-/-}$ (G and H) mice (n = 4–6 per group). Adipocyte size measurements were done on two sections per mouse.

(I and J) Infrared eye temperature readings during 12-hr cold exposure of AL and CR *Stat6*$^{-/-}$ (I) and *Il4ra*$^{+/+}$ and *Il4ra*$^{-/-}$ (J) mice (n = 4–6 per group) are shown. Error bars show mean ± SD. Significance was calculated using non-paired two-tailed Student's t test (*p ≤ 0.05, **p ≤ 0.01, and ***p ≤ 0.001).

overall adiposity, these results suggest that, at least in part, the ingSAT loss during CR is mediated by the browning of this tissue, unlike the pgVAT where browning is not as pronounced. CR on the BALB/c control mice, on the other hand, led to similar improvements in the tolerance to glucose and the sensitivity to insulin (Figures 5C and 5G) compared to the CR mice on the C57BL/6J background. As mentioned above, the fat depots of the BALB/c CR mice also had decreased weight (Figure 5J) and showed increased macrophage levels compared to the AL controls (Figure 6A). Accordingly, CR increased the expression of the browning markers in the fat depots of the BALB/c mice, and their adipocytes showed a multilocular appearance (Figures 6C–6E), demonstrating that CR leads to the development of beige fat irrespective of the genetic background of the mice. Consistent with the suppressed browning, neither CR *Stat6*-KO nor *Il4ra*-KO mice showed improvement in the tolerance to cold (Figures 6I, 6J, and S6F–S6J), while the energy expenditure of the CR *Stat6*-KO was lower than CR WT controls (Figure S6K). Together, this demonstrates that the increased browning and glucose phenotypes after CR are mediated by

increased type 2 immune signaling, irrespective of the genetic background of the mice.

Several of the metabolic improvements during the CR are in part mediated by the silent information regulator T1 Sirtuin1 (SIRT1) (Cantó and Auwerx, 2009). This NAD^+-dependent histone deacetylase plays an important role in regulating energy homeostasis in several metabolic tissues (Rodgers et al., 2008), linking the metabolic status to the transcriptional regulation. We therefore investigated its expression levels and found that SIRT1 was increased after CR in the visceral fat, and it was bordering statistical significance in the ingSAT (Figures S7A and S7B). Interestingly, SIRT1 levels were increased in both the eosinophils and macrophages present in the ingSAT, and the increment observed in the macrophages was due to its increased levels in the M2 polarized cells (Figures 7A, 7B, and S7C). SIRT1 deletion in macrophages results in increased transcription of proinflammatory target genes, while myeloid cell-specific SIRT1 knockout mice challenged with a high-fat diet display high levels of activated macrophages (M1) in liver and adipose tissue, predisposing the animals to the development of systemic insulin resistance and metabolic derangements (Schug et al., 2010). Increased SIRT1 levels also were present in the adipocytes isolated from both fat depots, as well as in the pgVAT macrophages (Figures S7D–S7F). Together, these data demonstrate that the increased SIRT1 expression is associated with the alternatively activated macrophages in the ingSAT following CR. In context of the SIRT1 role in regulating the macrophage polarization, these observations could point to this transcriptional factor as a possible upstream regulator of some of the beneficial effects following CR mediated by the type 2 immunity. Consistent with this idea, treatment of myeloid-derived suppressor cells with IL-4 increases the *Sirt1* expression (Liu et al., 2014), while the transgenic mice overexpressing SIRT1 are leaner, metabolically more active, and show improved glucose tolerance (Bordone et al., 2007), closely resembling the phenotype of the CR mice.

To further investigate the link between the immune signaling and the metabolic phenotype, we transplanted bone marrow-derived cells from the S*tat6*-KO donor mice to lethally irradiated WT or S*tat6*-KO recipients (WT bone marrow transplantation [BMT]^{KO} or KO BMT^{KO}, respectively), and we used WT donor transplantations to irradiated WT or S*tat6*-KO recipients as controls (WT BMT^{WT} or KO BMT^{WT}, respectively) (Figure S7G). While we could detect no changes in the glucose tolerance when transplanting the bone marrow-derived cells from the WT or S*tat6*-KO to AL-fed mice (Figure 7C), subjecting the transplanted mice to CR led to improved tolerance to glucose in all the animals transplanted with bone marrow-derived cells from the WT mice, when compared to the ones transplanted with *Stat6*-KO bone marrow-derived cells (Figures 7D and 7E). These improvements were irrespective of whether the recipient mice were S*tat6*-KO or WT. Similarly, both WT BMT^{WT} and KO BMT^{WT} CR mice showed improved insulin sensitivity compared to the WT BMT^{KO} and KO BMT^{KO} CR, while no changes were found in the AL-fed animals (Figures 7F–7H). Notably, CR led to decreased ingSAT weight only in the mice transplanted with bone marrow derived from WT mice (Figure 7I), suggesting a key contribution of the BM-derived cells to the metabolic improvements and the inSAT loss during CR. These observations were consistent with the smaller multilocular adipocytes present in the WT BMT^{WT} and KO BMT^{WT} CR mice (Figure 7J) and the higher expression of the key browning markers and increased eosinophil number in these animals, compared to CR WT BMT^{KO} and KO BMT^{KO} and AL WT BMT^{WT} and KO BMT^{WT} mice in both ingSAT and pgVAT depots (Figures 7K and S7H–S7L). These data demonstrate that the immune-competent bone marrow-derived cells mediate the browning phenotype and a number of metabolic improvements of the CR mice.

DISCUSSION

Long-term CR without malnutrition or intermittent fasting prolong the lifespan of yeast, plants, worms, flies, and rodents and also may have beneficial effects on longevity in primates. CR increases the health span and reduces the incidence of metabolic diseases, cancer, arteriosclerosis, and neurodegeneration. In rodents, the CR caused by a continuously low calorie intake, but not by intermittent fasting regimens, reduces the body weight and the total fat amount. Our data suggest that, at least in part, this overall decrease in the total fat during CR is due to the increased browning of the white fat depots. This is concomitant with increased eosinophils and M2 macrophage infiltration and with enhanced type 2 cytokine signaling in the fat tissues of the CR animals.

Genetic ablation of the type 2 immunity impaired the CR-induced browning of both white fat depots and suppressed the improved glucose tolerance and insulin sensitivity of the CR mice. Intriguingly, the subcutaneous fat loss in these CR KO mice was completely abrogated, suggesting that the decrease of this tissue during CR is enabled by the type 2 signaling. Suppression of the type 2 immunity, on the other hand, did not affect the visceral fat loss, consistent with the lower browning capacity of this fat depot. These results demonstrate that the increased type 2 signaling and the innate immunity are of key importance for a number of metabolic improvements during CR. In contrast to the cold exposure (Lee et al., 2015), CR did not affect the levels of the ILC2 cells, suggesting alternative upstream mechanisms contributing to the increased eosinophil and M2 levels.

SIRT1 is a histone deacetylase that affects the energy homeostasis in several metabolic tissues. The levels of SIRT1 were markedly increased in the alternatively activated macrophages, but they were not changed in the M1 polarized cells. It is well established that SIRT1 favors the M2 macrophage polarization, in agreement with the idea that its increased levels after CR might mediate some of the beneficial metabolic effects of CR that are linked to the innate immunite response. IL-4 increases the *Sirt1* expression (Liu et al., 2014) in vitro, raising the possibility that increased secretion of this type 2 cytokine promotes alternative macrophage activation, at least in part, through SIRT1. Accordingly, the increased expression of SIRT1 in vivo favors a leaner and metabolically healthier phenotype (Bordone et al., 2007), mirroring the metabolic benefits of the CR treatment.

Browning of the fat depots enhances energy dissipation and reduces the overall adiposity, thereby contributing to the overall fat decrease during CR. Cold exposure and long-term endurance exercise are physiological stimuli that increase the browning (van Marken Lichtenbelt et al., 2009; Harms and Seale, 2013; Wu et al., 2012, 2013; Boström et al., 2012). The increased

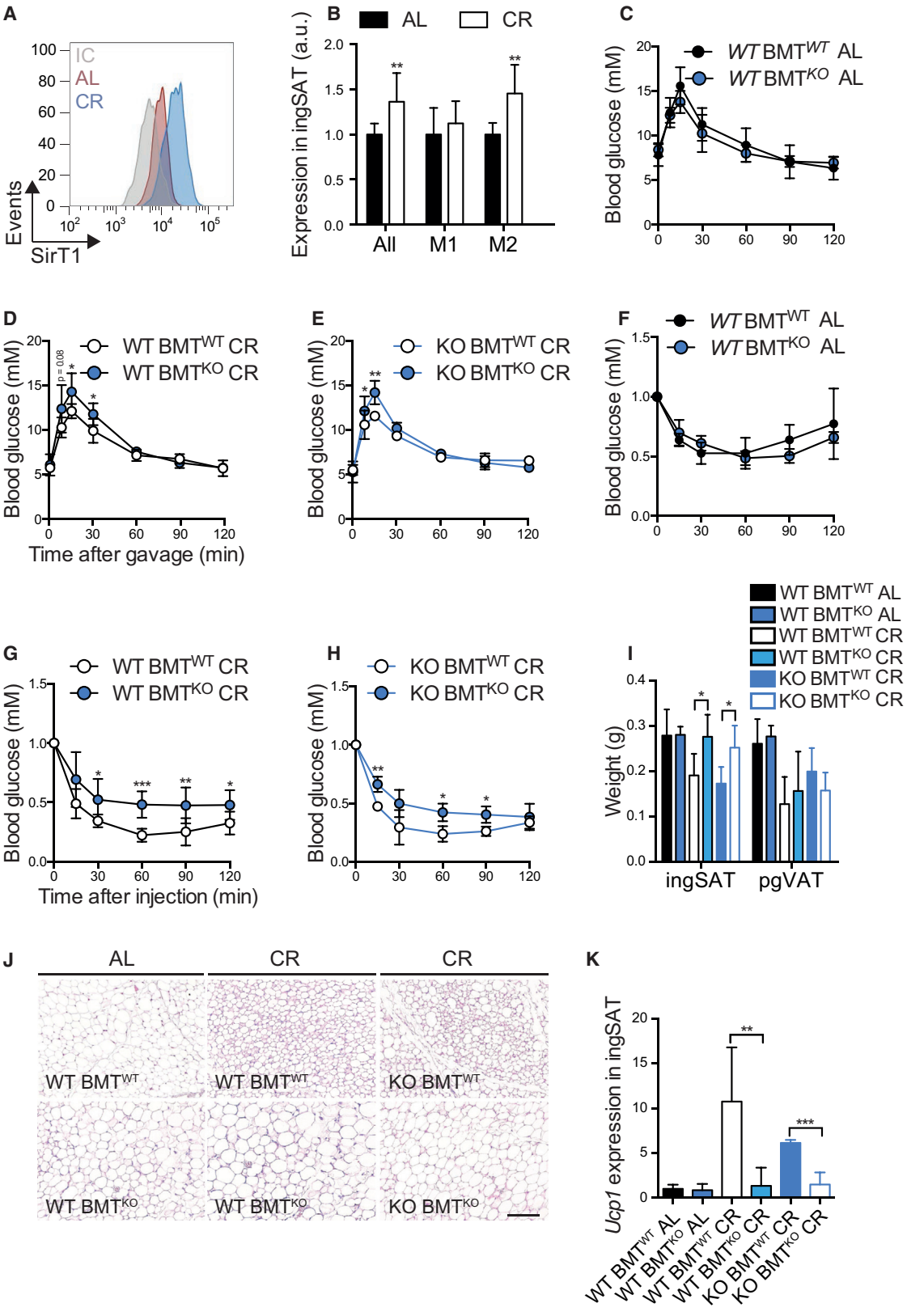

(legend on next page)

energy dissipation during cold exposure is physiologically justified by the need for increased heat production as a defense against hypothermia. The increased browning during exercise, on the other hand, seems paradoxical, and one explanation was that it might have evolved as a consequence of muscle contraction during shivering (Boström et al., 2012). We note that a common feature between the cold exposure and endurance exercise is the negative energy balance: higher energy expenditure than intake leading to fat loss. In addition, interventional microbiota depletion, either by means of antibiotics administration or in germ-free mice (Suárez-Zamorano et al., 2015; Chevalier et al., 2015), as well as RYGB (Neinast et al., 2015) also increase the browning to a similar extent as several endurance exercise regimens. These are also conditions of decreased caloric uptake and negative energy balance. Seen in this context, our results that CR promotes the development of functional beige fat provide insights into the regulation of the overall energy homeostasis during energy scarcity, and they suggest that white fat browning is a common feature of conditions of negative energy balance.

EXPERIMENTAL PROCEDURES

Animals

Cd45.1^{+} mice, *Stat6*$^{-/-}$ and *Il4ra*$^{-/-}$ mice, and their respective C57BL/6J and BALB/c controls were purchased from Charles River; *ob/ob* and their C57BL/6J controls were acquired from Janvier Labs. Mice were kept in a specific pathogen-free facility (SPF) in 12-hr day and night cycles and were fed standard chow diet (16.2 MJ/kg Gross Energy; 12.8 MJ/kg Metabolizable Energy; 9 kJ% Fat, 33 kJ% Protein, 58 kJ% Carbohydrates, V1534-727, Ssniff) or 60% calorie-restricted diet (CRD) (14.6 MJ/kg Gross Energy; 7.7 MJ/kg Metabolizable Energy; 11 kJ% Fat, 51 kJ% Protein, 38 kJ% Carbohydrates, S9631-S710, Ssniff). Animals were fed daily between 18 and 19 hr. Animals under chow diet CR received 40% less food than the average eaten by age-matched AL-fed mice. Mice on CRD received and consumed 30% more of the 60% calorie restricted diet daily, compared to AL fed controls, to obtain total of 20% CR. Cold and thermoneutral exposures were performed at 6°C and 30°C, respectively, in a light- and humidity-controlled climatic chamber (TSE) in SPF conditions. All experiments were started on male, 8-week-old mice, unless otherwise stated. Weight-matched (WM) controls for CR animals were 5–8 weeks old. Upon arrival animals were allocated to groups based on their body weight to ensure equal starting points. All mice were sacrificed after 5 hr fasting. Blood (500 μL) was taken from terminally anesthetized mice in tubes with 11 μL 0.5 mM EDTA, 2 μL aprotinin, and 2 μL DPPIV and plasma stored at −80°C. All animal experiments were approved by the Swiss federal and Geneva cantonal authorities for animal experimentation (Office vétérinaire federal and Comission cantonale pour les expériences sur les animaux de Genève).

BMTs

The 8-week-old recipient WT CD45.1 and *Stat6*$^{-/-}$ mice (which possess the CD45.2 variant) were lethally irradiated with 1,000 rad. Then 24 hr later, animals were reconstituted via tail vein injection with 5 × 10^{6} bone marrow hematopoietic cells collected from donor *Stat6*$^{-/-}$ or C57BL/6J mice. Mice were treated with Baytril 10% (6 mL/L drinking water) for the following 2 weeks. Five weeks after tail vein injection, the reconstitution was confirmed by analyzing the presence of CD45.1 or CD45.2 in peripheral blood of recipient mice. Animals were subsequently kept AL fed or submitted to CR following the described protocol.

PET-CT

Mice were anesthetized with 2% isoflurane and were injected in the venous sinus with 5–6 megabecquerel (MBq) [^{18}F]FDG. Mice were then left awake at RT during the uptake time of 20 min. Then 10 min prior to PET scan, mice were subjected to CT scans in a Triumph microPET/SPECT/CT system (TriFoil). Images were obtained at 80 peak kilovoltage (kVp) and 160 μA, and 1,024 projections were acquired during the 360° rotation with a field of view of 71.3 mm (1.7× magnification). After 20 min of [^{18}F]FDG uptake, PET scans were started for a total duration of 10 min.

PET scans were reconstructed with the built-in LabPET software using an OSEM3D (20 iterations) algorithm, and images were calibrated in Bq per milliliter by scanning a phantom cylinder. The Triumph XO software, which uses a back-projection engine, was used to reconstruct the CT scans with a matrix of 512 and a voxel size of 0.135 mm. CT scans were co-registered with the PET scans using the plugin Vivid (TriFoil) for Amira (FEI) and exported as dicom files. The software Osirix (Pixmeo) was used to quantitatively analyze the datasets and generate pictures. Regions of interest (ROIs) were drawn on contiguous slices on CT scans and computed as 3D volumes for the measurements of volumes and densities of the indicated adipose tissues. Then, PET series were converted to display standardized uptake values (SUVs) adjusted to the body weight of the animals and merged with CT sets. 3D ROIs derived from CT scans were used to quantify the uptake of [^{18}F]FDG in the indicated adipose tissues.

Flow Cytometry and the Characterization of Hematopoietic Cell Populations

Primary stromal vascular fractions (SVFs) from adipose tissues were prepared as described (Sun and Trajkovski, 2014; Trajkovski et al., 2012). Single-cell preparations were washed in PBS supplemented with 0.1% BSA and 0.5 mM EDTA (pH 8.0), and they were stained with rat monoclonal anti-F4/80 (clone A3-1, ab105155, 1:200, Abcam), rat monoclonal anti-CD11b (clone M1/70, 561114, 1:200, BD Biosciences), rat monoclonal anti-CD301 (MGL1/MGL2) (clone LOM-14, 145705, 1:400, BioLegend), and hamster monoclonal anti-CD11c (clone N418, 117330, 1:200, BioLegend) for macrophage stainings; rat monoclonal anti-CD45 (clone 104, 558702, 1:200, BD Biosciences) or rat monoclonal anti-CD11b (clone M1/70, 561114, 1:200, BD Biosciences) and rat monoclonal anti-Siglec F (clone E50-2440, 562068, 1:200, BD Biosciences) for eosinophil staining; rat monoclonal anti-CD45 (clone 104, 558702, 1:200, BD Biosciences), mouse hematopoietic lineage cocktail (22-7770, 1:200, eBioscience), rat monoclonal anti-CD25 (clone PC61, 1:200, BD Biosciences), and rat monoclonal anti-ST2 (IL-33R, clone RMST2-2, 46-9335, 1:200, eBioscience) for ILC2 cells; and rat monoclonal anti-CD4 (clone RM4-5, 48-0042, 1:200, eBioscience) or rat monoclonal anti-CD8 (clone 53-6.7, 12-0081, 1:200, eBioscience) for CD4 and CD8 T cells, respectively.

When appropriate, cells were subsequently washed again twice before being acquired. For intracellular stainings, cells were fixed in 4% paraformaldehyde, then labeled with rat monoclonal anti-NOS2 (clone CXNFT, 61-5920,

Figure 7. CR-Induced Browning Relies on Competent Immune Response

(A) SIRT1 protein expression in CD11b^{+}F4/80^{+} macrophages in ingSAT of AL and CR mice. In gray, the isotype control (IC) is shown.

(B) Quantification of SIRT1 protein levels in total, M1, or M2 macrophages within the ingSAT of AL and CR mice (n = 8–10 per group) is shown.

(C–H) OGTT (C–E) and insulin tolerance test (F–H) of WT *Stat6*$^{+/+}$ (WT, CD45.1^{+}) (C, D, F, and G) and *Stat6*-KO (KO, CD45.2^{+}) (E and H) mice lethally irradiated and subsequently transplanted with bone marrow hematopoietic cells from WT (WT BMT^{WT} or KO BMT^{WT}, respectively) or *Stat6*-KO (WT BMT^{KO} or KO BMT^{KO}, respectively) and kept AL (C and F) or under CR (D, E, G, and H) (n = 5–9 per group) are shown.

(I) Organ weights of mice as in (C–H) (n = 5–9 per group) are shown.

(J) Representative H&E-stained histological sections from ingSAT of lethally irradiated AL and CR WT and KO mice, reconstituted with WT (top line, BMT^{WT}) or KO (bottom line, BMT^{KO}) hematopoietic cells as in (C–H), are shown.

(K) Relative Ucp1 mRNA expression in ingSAT of AL and CR mice as in (A) (n = 5–9 per group) is shown.

Scale bars, 200 μm. Error bars show mean ± SD. Significance was calculated using non-paired two-tailed Student's t test (*p ≤ 0.05, **p ≤ 0.01, and ***p ≤ 0.001).

eBioscience), sheep polyclonal anti-Arg1 (IC5868P, R&D Systems), rabbit monoclonal anti-TH (clone EP1533Y, TA303716, 1:50, Origene), rabbit polyclonal anti SirT1 (mouse specific, 2028, 1:100, Cell Signaling Technology), or rabbit mAB isotype control (3900, 1:100, Cell Signaling Technology), followed by polyclonal goat anti-rabbit secondary antibody (A-10931, 1:400, Thermo Fisher Scientific) in permeabilization buffer (PBS with 0.5% Tween 20). Data were acquired using a Gallios Flow Cytometer (Beckman Coulter) and analyzed with FlowJo v10 software. After gating out dead cells and doublets, macrophages were identified as $CD11b^+F4/80^+$, eosinophils as $CD11b^+$ Siglec-F^+ cells, and ILC2 as $Lin^-CD45^+CD25^+IL33R^+$ cells.

Statistics

Unless otherwise specified in the figure legends, significance was calculated using non-paired two-tailed Student's t test. For all figures, $^*p \leq 0.05$, $^{**}p \leq 0.01$, and $^{***}p \leq 0.001$. Errors represent SD unless otherwise stated. Sample sizes and animal numbers were chosen based on power calculations of 0.8. All experiments were independently performed at least three times without blinding, and representative values from one experiment are shown. No animals or values were excluded from the analysis.

SUPPLEMENTAL INFORMATION

Supplemental Information includes Supplemental Experimental Procedures and seven figures and can be found with this article online at http://dx.doi.org/10.1016/j.cmet.2016.07.023.

AUTHOR CONTRIBUTIONS

S.F. designed and performed experiments, developed the hypothesis, analyzed data, and prepared figures. N.S.-Z., D.R., C.V.-D., and A.S.D. participated in experiments. D.J.C. helped with the PET-CT experiments. M.T. initiated, designed, and supervised the work; developed the hypothesis; analyzed data; and wrote the manuscript with input from all authors.

ACKNOWLEDGMENTS

We thank M. Gustafsson Trajkovska, C. Wollheim, and R. Coppari for discussions and critical reading of the manuscript; S. Germain for help with the PET-CT; J. Niven and K. Steinbach for technical help; J.-C. Martinou for help with the Seahorse analyzer; and G. Waksman for support. The research leading to these results has received funding from the European Research Council (ERC) under the European Union's Seventh Framework Programme (FP/2007-2013)/ERC Grant Agreement 336607 (ERC-2013-StG-336607), the Louis-Jeantet Foundation, the Fondation pour Recherches Médicales, the Novartis Foundation (14B053), and the Swiss National Science Foundation (SNSF) Professorship (PP00P3_144886) to M.T.

Received: February 26, 2016
Revised: June 22, 2016
Accepted: July 26, 2016
Published: August 25, 2016

REFERENCES

Barzilai, N., and Gabriely, I. (2001). The role of fat depletion in the biological benefits of caloric restriction. J. Nutr. *131*, 903S–906S.

Barzilai, N., Banerjee, S., Hawkins, M., Chen, W., and Rossetti, L. (1998). Caloric restriction reverses hepatic insulin resistance in aging rats by decreasing visceral fat. J. Clin. Invest. *101*, 1353–1361.

Bianco, A.C., and Silva, J.E. (1987). Intracellular conversion of thyroxine to triiodothyronine is required for the optimal thermogenic function of brown adipose tissue. J. Clin. Invest. *79*, 295–300.

Bordone, L., and Guarente, L. (2005). Calorie restriction, SIRT1 and metabolism: understanding longevity. Nat. Rev. Mol. Cell Biol. *6*, 298–305.

Bordone, L., Cohen, D., Robinson, A., Motta, M.C., van Veen, E., Czopik, A., Steele, A.D., Crowe, H., Marmor, S., Luo, J., et al. (2007). SIRT1 transgenic mice show phenotypes resembling calorie restriction. Aging Cell *6*, 759–767.

Boström, P., Wu, J., Jedrychowski, M.P., Korde, A., Ye, L., Lo, J.C., Rasbach, K.A., Boström, E.A., Choi, J.H., Long, J.Z., et al. (2012). A PGC1-α-dependent myokine that drives brown-fat-like development of white fat and thermogenesis. Nature *481*, 463–468.

Cannon, B., and Nedergaard, J. (2004). Brown adipose tissue: function and physiological significance. Physiol. Rev. *84*, 277–359.

Cantó, C., and Auwerx, J. (2009). Caloric restriction, SIRT1 and longevity. Trends Endocrinol. Metab. *20*, 325–331.

Cantó, C., and Auwerx, J. (2011). Calorie restriction: is AMPK a key sensor and effector? Physiology (Bethesda) *26*, 214–224.

Chevalier, C., Stojanović, O., Colin, D.J., Suarez-Zamorano, N., Tarallo, V., Veyrat-Durebex, C., Rigo, D., Fabbiano, S., Stevanović, A., Hagemann, S., et al. (2015). Gut microbiota orchestrates energy homeostasis during cold. Cell *163*, 1360–1374.

Colman, R.J., Beasley, T.M., Kemnitz, J.W., Johnson, S.C., Weindruch, R., and Anderson, R.M. (2014). Caloric restriction reduces age-related and all-cause mortality in rhesus monkeys. Nat. Commun. *5*, 3557.

Cousin, B., Cinti, S., Morroni, M., Raimbault, S., Ricquier, D., Pénicaud, L., and Casteilla, L. (1992). Occurrence of brown adipocytes in rat white adipose tissue: molecular and morphological characterization. J. Cell Sci. *103*, 931–942.

De Guzman, J.M., Ku, G., Fahey, R., Youm, Y.H., Kass, I., Ingram, D.K., Dixit, V.D., and Kheterpal, I. (2013). Chronic caloric restriction partially protects against age-related alteration in serum metabolome. Age (Dordr.) *35*, 1091–1104.

Feldmann, H.M., Golozoubova, V., Cannon, B., and Nedergaard, J. (2009). UCP1 ablation induces obesity and abolishes diet-induced thermogenesis in mice exempt from thermal stress by living at thermoneutrality. Cell Metab. *9*, 203–209.

Ferguson, M., Sohal, B.H., Forster, M.J., and Sohal, R.S. (2007). Effect of long-term caloric restriction on oxygen consumption and body temperature in two different strains of mice. Mech. Ageing Dev. *128*, 539–545.

Ganeshan, K., and Chawla, A. (2014). Metabolic regulation of immune responses. Annu. Rev. Immunol. *32*, 609–634.

Ghorbani, M., Claus, T.H., and Himms-Hagen, J. (1997). Hypertrophy of brown adipocytes in brown and white adipose tissues and reversal of diet-induced obesity in rats treated with a beta3-adrenoceptor agonist. Biochem. Pharmacol. *54*, 121–131.

Guerra, C., Koza, R.A., Yamashita, H., Walsh, K., and Kozak, L.P. (1998). Emergence of brown adipocytes in white fat in mice is under genetic control. Effects on body weight and adiposity. J. Clin. Invest. *102*, 412–420.

Harms, M., and Seale, P. (2013). Brown and beige fat: development, function and therapeutic potential. Nat. Med. *19*, 1252–1263.

Himms-Hagen, J., Melnyk, A., Zingaretti, M.C., Ceresi, E., Barbatelli, G., and Cinti, S. (2000). Multilocular fat cells in WAT of CL-316243-treated rats derive directly from white adipocytes. Am. J. Physiol. Cell Physiol. *279*, C670–C681.

Kelley, D.E., Wing, R., Buonocore, C., Sturis, J., Polonsky, K., and Fitzsimmons, M. (1993). Relative effects of calorie restriction and weight loss in noninsulin-dependent diabetes mellitus. J. Clin. Endocrinol. Metab. *77*, 1287–1293.

Kopecky, J., Clarke, G., Enerbäck, S., Spiegelman, B., and Kozak, L.P. (1995). Expression of the mitochondrial uncoupling protein gene from the aP2 gene promoter prevents genetic obesity. J. Clin. Invest. *96*, 2914–2923.

Lee, M.W., Odegaard, J.I., Mukundan, L., Qiu, Y., Molofsky, A.B., Nussbaum, J.C., Yun, K., Locksley, R.M., and Chawla, A. (2015). Activated type 2 innate lymphoid cells regulate beige fat biogenesis. Cell *160*, 74–87.

Liu, G., Bi, Y., Shen, B., Yang, H., Zhang, Y., Wang, X., Liu, H., Lu, Y., Liao, J., Chen, X., and Chu, Y. (2014). SIRT1 limits the function and fate of myeloid-derived suppressor cells in tumors by orchestrating HIF-1α-dependent glycolysis. Cancer Res. *74*, 727–737.

Lowell, B.B., S-Susulic, V., Hamann, A., Lawitts, J.A., Himms-Hagen, J., Boyer, B.B., Kozak, L.P., and Flier, J.S. (1993). Development of obesity in transgenic mice after genetic ablation of brown adipose tissue. Nature *366*, 740–742.

Martinez, F.O., Helming, L., and Gordon, S. (2009). Alternative activation of macrophages: an immunologic functional perspective. Annu. Rev. Immunol. *27*, 451–483.

Neinast, M.D., Frank, A.P., Zechner, J.F., Li, Q., Vishvanath, L., Palmer, B.F., Aguirre, V., Gupta, R.K., and Clegg, D.J. (2015). Activation of natriuretic peptides and the sympathetic nervous system following Roux-en-Y gastric bypass is associated with gonadal adipose tissues browning. Mol. Metab. *4*, 427–436.

Nguyen, K.D., Qiu, Y., Cui, X., Goh, Y.P., Mwangi, J., David, T., Mukundan, L., Brombacher, F., Locksley, R.M., and Chawla, A. (2011). Alternatively activated macrophages produce catecholamines to sustain adaptive thermogenesis. Nature *480*, 104–108.

Ocampo, A., Liu, J., Schroeder, E.A., Shadel, G.S., and Barrientos, A. (2012). Mitochondrial respiratory thresholds regulate yeast chronological life span and its extension by caloric restriction. Cell Metab. *16*, 55–67.

Qiang, L., Wang, L., Kon, N., Zhao, W., Lee, S., Zhang, Y., Rosenbaum, M., Zhao, Y., Gu, W., Farmer, S.R., and Accili, D. (2012). Brown remodeling of white adipose tissue by SirT1-dependent deacetylation of Pparγ. Cell *150*, 620–632.

Qiu, Y., Nguyen, K.D., Odegaard, J.I., Cui, X., Tian, X., Locksley, R.M., Palmiter, R.D., and Chawla, A. (2014). Eosinophils and type 2 cytokine signaling in macrophages orchestrate development of functional beige fat. Cell *157*, 1292–1308.

Rodgers, J.T., Lerin, C., Gerhart-Hines, Z., and Puigserver, P. (2008). Metabolic adaptations through the PGC-1 alpha and SIRT1 pathways. FEBS Lett. *582*, 46–53.

Schug, T.T., Xu, Q., Gao, H., Peres-da-Silva, A., Draper, D.W., Fessler, M.B., Purushotham, A., and Li, X. (2010). Myeloid deletion of SIRT1 induces inflammatory signaling in response to environmental stress. Mol. Cell. Biol. *30*, 4712–4721.

Silva, J.E. (1988). Full expression of uncoupling protein gene requires the concurrence of norepinephrine and triiodothyronine. Mol. Endocrinol. *2*, 706–713.

Stanford, K.I., Middelbeek, R.J., Townsend, K.L., An, D., Nygaard, E.B., Hitchcox, K.M., Markan, K.R., Nakano, K., Hirshman, M.F., Tseng, Y.H., and Goodyear, L.J. (2013). Brown adipose tissue regulates glucose homeostasis and insulin sensitivity. J. Clin. Invest. *123*, 215–223.

Suárez-Zamorano, N., Fabbiano, S., Chevalier, C., Stojanović, O., Colin, D.J., Stevanović, A., Veyrat-Durebex, C., Tarallo, V., Rigo, D., Germain, S., et al. (2015). Microbiota depletion promotes browning of white adipose tissue and reduces obesity. Nat. Med. *21*, 1497–1501.

Sun, L., and Trajkovski, M. (2014). MiR-27 orchestrates the transcriptional regulation of brown adipogenesis. Metabolism *63*, 272–282.

Trajkovski, M., Ahmed, K., Esau, C.C., and Stoffel, M. (2012). MyomiR-133 regulates brown fat differentiation through Prdm16. Nat. Cell Biol. *14*, 1330–1335.

van Marken Lichtenbelt, W.D., Vanhommerig, J.W., Smulders, N.M., Drossaerts, J.M., Kemerink, G.J., Bouvy, N.D., Schrauwen, P., and Teule, G.J. (2009). Cold-activated brown adipose tissue in healthy men. N. Engl. J. Med. *360*, 1500–1508.

Wei, M., Fabrizio, P., Hu, J., Ge, H., Cheng, C., Li, L., and Longo, V.D. (2008). Life span extension by calorie restriction depends on Rim15 and transcription factors downstream of Ras/PKA, Tor, and Sch9. PLoS Genet. *4*, e13.

Wu, D., Molofsky, A.B., Liang, H.E., Ricardo-Gonzalez, R.R., Jouihan, H.A., Bando, J.K., Chawla, A., and Locksley, R.M. (2011). Eosinophils sustain adipose alternatively activated macrophages associated with glucose homeostasis. Science *332*, 243–247.

Wu, J., Boström, P., Sparks, L.M., Ye, L., Choi, J.H., Giang, A.H., Khandekar, M., Virtanen, K.A., Nuutila, P., Schaart, G., et al. (2012). Beige adipocytes are a distinct type of thermogenic fat cell in mouse and human. Cell *150*, 366–376.

Wu, J., Cohen, P., and Spiegelman, B.M. (2013). Adaptive thermogenesis in adipocytes: is beige the new brown? Genes Dev. *27*, 234–250.

Young, P., Arch, J.R., and Ashwell, M. (1984). Brown adipose tissue in the parametrial fat pad of the mouse. FEBS Lett. *167*, 10–14.